Spectrochimica Acta Part A: Molecular and Biomolecular Spectroscopy 127 (2014) 74–84

Contents lists available at ScienceDirect

Spectrochimica Acta Part A: Molecular and Biomolecular Spectroscopy

journal homepage: www.elsevier.com/locate/saa

Synthesis, crystal structure, conformational and vibrational properties of 6-acetyl-2,2-dimethyl-chromane

Emilio Lizarraga [a,1], Diego M. Gil [a,1], Gustavo A. Echeverría [c], Oscar E. Piro [c], César A.N. Catalán [b], Aída Ben Altabef [a,*]

[a] INQUINOA, CONICET, Instituto de Química Física, Facultad de Bioquímica, Química y Farmacia, Universidad Nacional de Tucumán, San Lorenzo 456, T4000CAN Tucumán, Argentina
[b] INQUINOA, CONICET, Instituto de Química Orgánica, Facultad de Bioquímica, Química y Farmacia, Universidad Nacional de Tucumán, Ayacucho 471, T4000INI Tucumán, Argentina
[c] Departamento de Física, Facultad de Ciencias Exactas, Universidad Nacional de La Plata and Institute IFLP (CONICET, CCT-La Plata), C.C. 67, 1900 La Plata, Argentina

HIGHLIGHTS

- The 6-acetyl-2,2-dimethyl-chromane compound was synthesized and characterized.
- The crystal structure was determined by single-crystal X-ray diffraction methods.
- The vibrational frequencies and ^{1}H NMR chemical shifts have been calculated and compared with the experimental data.
- HOMO, LUMO and UV–Visible spectral analysis have been used to elucidate the electronic transitions.
- DSC measurements were performed in order to determine the thermodynamic parameters associated to different transitions.

GRAPHICAL ABSTRACT

Unit cell content and Infrared and Raman spectra of 6-acetyl-2,2-dimethyl-chromane.

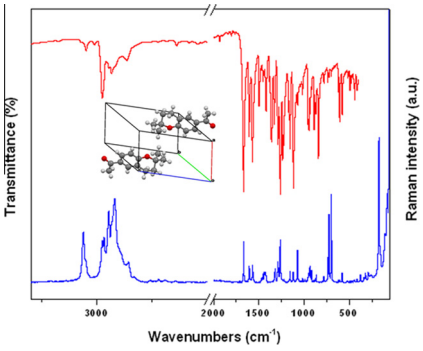

ARTICLE INFO

Article history:
Received 19 December 2013
Received in revised form 4 February 2014
Accepted 14 February 2014
Available online 24 February 2014

Keywords:
6-Acetyl-2,2-dimethyl-chromane
DFT calculations
IR and Raman spectroscopy
NBO analysis
X-ray crystal structure determination

ABSTRACT

The 6-acetyl-2,2-dimethyl-chromane compound was synthesized and characterized by IR, Raman, UV–Visible and ^{1}H NMR spectroscopies. Its solid state structure was determined by X-ray diffraction methods. The substance crystallizes in the triclinic *P*-1 space group with $a = 5.9622(5)$ Å, $b = 10.342(1)$ Å, $c = 10.464(1)$ Å, $\alpha = 63.81(1)°$, $\beta = 81.923(9)°$, $\gamma = 82.645(9)°$, and $Z = 2$ molecules per unit cell. Due to extended π-bonding delocalization a substantial skeletal fragment of the molecule is planar. The vibrational modes were calculated at B3LYP/6-31G(d,p) level and all of them assigned in the IR and Raman spectra. The DFT calculated ^{1}H NMR spectrum (chemical shifts) were in good agreement with the experimental data. The electronic (UV–Visible) spectrum was calculated using TD-DFT method in gas phase and it was correlated with the experimental data. The assignment and analysis of the frontier HOMO and LUMO orbitals indicate that the absorption bands are mainly originated from $\pi \rightarrow \pi^*$ transitions. According to DSC measurements the substance presents a melting point of 93 °C and decomposes at temperatures higher than 196 °C.

* Corresponding author. Tel.: +54 381 4311044; fax: +54 381 4248169.
E-mail address: altabef@fbqf.unt.edu.ar (A. Ben Altabef).
[1] These two authors contributed equally to this paper.

http://dx.doi.org/10.1016/j.saa.2014.02.035
1386-1425/

Introduction

As is well-known, hetero-cycles compounds are widespread in natural products and have attracted considerable attention from a wide area of science, including physical chemistry, medicinal chemistry, natural product chemistry, synthetic organic chemistry and polymer science [1].

4-Hydroxi-3-(3-methyl-2-butenyl)-acetophenone is the main secondary matebolite from *Senecio nutans*, a medicinal plant of Asteraceae family [2]. Moreover, the prenyled p-hydroxyacetophenone derivatives are important biogenetic precursors of benzofurans and benzochromenes, two significant groups of bioactive metabolites in the plant kingdom [3].

Chromane and chromene substructures are frequently found in naturally occurring compounds, many of which exhibit useful biological activity [4,5]. Several biologically active chromenes and chromanes have been isolated from several natural sources. These compounds are characterized by different biological properties such as antibacterial [6,7], antifungal [8], trypanocidal [9], apoptosis-inducing agents [10,11], anti-HIV agents [12,13], and modulators of estrogen receptors [14,15].

Here we report the synthesis and crystal structure of 6-acetyl-2,2-dimethyl-chromane by X-ray diffraction methods and its infrared, Raman and NMR spectra. Differential Scanning Calorimetry (DSC) measurements were also carried out to evaluate the enthalpy (ΔH) and entropy (ΔS) variations associated with different transitions. The molecular geometry optimizations were performed using DFT/B3LYP methods and different basis sets to assist the interpretation and the assignment of experimental IR and Raman spectra. Moreover, the crystal structure of the title compound was determinate by X-ray diffraction methods, and their experimental geometrical parameters were used to validate the theoretical results. The study was complemented with natural bond orbitals (NBO) analysis [16] and HOMO–LUMO studies to evaluate the nature of the rings and the electronic properties of the compound.

Experimental section

Isolation of 4-hydroxi-3-(3-methyl-2-butenyl)-acetophenone (1)

Compound **1** was obtained from an extract of *S. nutans* [2]. 114 g of methylene chloride extract was dissolved in ethyl ether (200 mL) and extracted with 7% NaOH (2 × 100 mL); the alkaline phase was washed with methylene chloride (2 × 10 mL) and then 31% HCl was added dropwise until pH 3 and extracted with methylene chloride (3 × 60 mL). The CH_2Cl_2 extracts were reunited and the solvent evaporated to yield 22.4 g of residue which was chromatographed on silica gel Merck 70–230 mesh using hexane–ethyl acetate 5:1 as elution solvent. Fractions showing a single spot on TLC were reunited and the solvent was evaporated to yield 13.4 g of compound **1** as a crystalline solid which was re-crystallized in ethanol–water 1:1, melting point (mp) 95–96 °C. The mp value obtained is similar to reported by Marchese et al. [17]; UV, EI-MS, ^{1}H and ^{13}C NMR spectra: identical to the reported previously [18–20].

Synthesis of 6-acetyl-2,2-dimethyl-chromane (2)

Compound **1** (1.5 g; 7.35 m mol) was dissolved in 40 mL of ethanol containing 4.5 mL of concentrated HCl (Scheme 1) and refluxed for 5 h. After cooling, 50 mL de distilled water was added and the resulting mixture was extracted with methylene chloride (3 × 50 mL). The organic extracts were reunited, washed with water (10 mL), 5% $NaHCO_3$ (3 × 20 mL) and brine (20 mL). After drying (Na_2SO_4) and solvent evaporation, 1.07 g (yield 72%) of crude **2** was obtained. Single crystals, adequate for structural X-ray diffraction measurements, were obtained from slow evaporation of ethanol–water (1:1) solutions. The melting point and the purity of the crystals obtained were 94–95 °C and 99.98% (GC), respectively. The purity was determined by capillary gas chromatography using both flame ionization detector (FID) and selective mass detector. EIMS: m/z (rel. int.) [M]+ 204 (52), 189 (82), 161 (26), 151 (11), 149 (100), 133 (40), 121 (6), 115 (6), 105 (8), 91 (16), 77 (22), 65 (7), 51 (12), 43 (57).

2.2 Instrumentation

Infrared and Raman spectroscopy

The room temperature (RT) infrared absorption spectrum of solid state 6-acetyl-2,2-dimethyl-chromane was recorded in the 4000–400 cm^{-1} frequency range with a Perkin–Elmer GX1 Fourier Transform infrared instrument. The Raman dispersion spectrum of the solid at RT was measured in the 3500 and 50 cm^{-1} interval with a Thermoscientific DXR Raman microscope. The Raman data were collected using a diode-pump, solid state laser of λ = 532 nm (at 5 cm^{-1} spectral resolution), a con-focal aperture of 25 μm pinhole and a 10× objective. The sample was placed on gold-coated sample slides. To achieve a sufficient signal to noise ratio, 30 spectral scans of 2 s each were accumulated during the measurements with the laser power maintained at 10 mW.

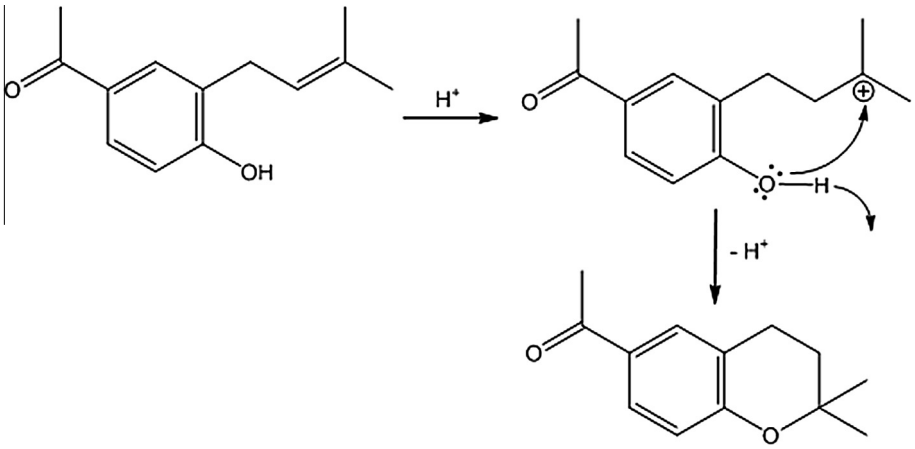

Scheme 1. Synthesis of 6-acetyl-2,2-dimethyl-chromane.

NMR spectra

^{1}H NMR was recorded on a Bruker AC (200 MHz) spectrometer. Sample was dissolved in $CDCl_3$ and tetramethyl silane (TMS) was used as internal standard. Chemical shifts were recorded in δ (ppm) values relative to TMS and J values are expressed in Hertz.

UV–Visible spectroscopy

UV–Visible measurements were recorded using quartz cells (10 mm optical path length) on an Shimadzu 160A spectrophotometer. For this purpose, a solution of 9.84 mg/L of compound **2** in ethanol 96° was prepared. The spectrum was recorder between 800 and 200 nm.

GC-MS measurements

The GC-MS analysis was carried out with a 5973 Hewlett Packard selective mass detector (quadrupole), source 70 eV, coupled to a HP 6890 GC fitted with a HP-5MS column (5% phenylmethyl siloxane, 30 m × 0.25 mm; film thickness 0.25 μm) with helium as carrier gas (1.0 mL/min; constant flow). The oven was programmed as follows: 150 °C (0 min), 150–180 °C (3 °C/min), 180 °C (2 min), 180–234 °C (1.5°/min), 234 °C (2 min). Injection: 0.1 μL of a 10% solution of the compound dissolved in methylene chloride. Injector and detector temperatures were maintained at 250 °C and 270 °C, respectively. Injection port was maintained at 250 °C, GC-MS inter-phase at 275 °C, ion source 230 °C, and MS Quad at 150 °C. The mass spectrum is shown in Fig. S1 (Supporting Information).

Differential Scanning Calorimetry (DSC)

Calorimetric measurements were performed using a differential scanning calorimeter Perkin Elmer Pyris DSC 6. The experiments were carried out using 1.150 mg of powdered sample sealed in aluminum pans with a mechanical crimp. Temperature and heat flow calibrations were made with standard samples of indium by using its melting transition. Enthalpy changes associated with the melting point of the sample in study (ΔH) were directly obtained from the DSC data by integrating the anomalous peak in the baseline subtracted curve. The entropy change relative to the phase transition was finally determined using the relationship $\Delta S = \Delta H/T$.

X-ray diffraction data

The measurements were performed on an Oxford Xcalibur Gemini, Eos CCD diffractometer with graphite-monochromated Cu Kα (λ = 1.54184 Å) radiation. X-ray diffraction intensities were collected (ω scans with ϑ and κ-offsets), integrated and scaled with CrysAlisPro [21] suite of programs. The unit cell parameters were obtained by least-squares refinement (based on the angular settings for all collected reflections with intensities larger than seven times the standard deviation of measurement errors) using CrysAlisPro. Data were corrected empirically for absorption employing the multi-scan method implemented in CrysAlisPro. The structure was solved by direct methods with SHELXS-97 [22] and the corresponding molecular model developed by alternated cycles of Fourier methods and full-matrix least-squares refinement on F^2 with SHELXL-97 [23]. All hydrogen atoms were located in a difference Fourier map phased on the heavier atoms and refined at their found positions with isotropic displacement parameters. The optimized methyl H-positions converged to staggered conformations. Crystal data and structure refinement results are summarized in Table 1. Crystallographic structural data have been deposited at the Cambridge Crystallographic Data Centre (CCDC). Any request to the Cambridge Crystallographic Data Centre for this material should quote the full literature citation and the reference number CCDC 977091.

Table 1
Crystal data and structure refinement results for 6-acetyl-2,2-dimethyl chromane.

Empirical formula	C_{13} H_{16} O_2	
Formula weight	204.26	
Temperature	293(2) K	
Wavelength	1.54184 Å	
Crystal system	Triclinic	
Space group	P-1	
Unit cell dimensions	a = 5.9622(5) Å	α = 63.81(1)°
	b = 10.342(1) Å	β = 81.923(9)°
	c = 10.464(1) Å	γ = 82.645(9)°
Volume	571.65(9) Å^3	
Z, Density (calculated)	2, 1.187 Mg/m^3	
Absorption coefficient	0.625 mm^{-1}	
F(000)	220	
Crystal size	0.502 × 0.277 × 0.179 mm^3	
2θ-range for data collection	4.73–71.96°	
Index ranges	$-7 \leqslant h \leqslant 4$, $-12 \leqslant k \leqslant 11$, $-12 \leqslant l \leqslant 12$	
Reflections collected	3796	
Independent reflections	2227 [R(int) = 0.0242]	
Observed reflections	1888	
Completeness to ϑ = 71.96°	99.1%	
Refinement method	Full-matrix least-squares on F^2	
Data/restraints/parameters	2227/0/201	
Goodness-of-fit on F^2	1.053	
Final R indices[a] [$I > 2\sigma(I)$]	R_1 = 0.0532, wR_2 = 0.1534	
R indices (all data)	R_1 = 0.0592, wR_2 = 0.1657	
Extinction coefficient	0.059(6)	
Largest diff. peak and hole	0.242 and −0.179 e Å^{-3}	

[a] $R_1 = \Sigma||F_o|-|F_c||/\Sigma|F_o|$, $wR_2 = [\Sigma w(|F_o|^2-|F_c|^2)^2/\Sigma w(|F_o|^2)^2]^{1/2}$.

2.3 Computational methods

Theoretical calculations were performed using the program package Gaussian 03 [24]. The potential energies associated with the C(8)C(7)C(1)C(6) dihedral angle were calculated at B3LYP level using the 6-31G(d,p) basis sets, with that torsion angle frozen and all other parameters allowed to relax. The total energy curves were sampled in steps of 10° using default convergence criteria as implemented in the Gaussian program [24]. Final optimizations and vibration frequency calculations were implemented employing the 6-31G(d,p) and 6-311++G(d,p) basis sets. The computed vibrational properties correspond, in all cases, to potential energy minima with no imaginary values for the frequencies.

A natural bond orbital (NBO) calculation was performed at the B3LYP/6-311++G(d,p) level using the program NBO 3.1 [16] as implemented in Gaussian 03 package. This analysis was performed to understand various second-order interactions between the filled orbitals of one subsystem and vacant orbitals of another subsystem. NBO analysis provides an efficient method for studying intra- and intermolecular interactions and also provides a convenient basis for investigating charge transfer or conjugative interaction in molecular systems. The calculated chemical shifts of the ^{1}H NMR spectrum was obtained by means of the GIAO method [25] using the B3LYP/6-311++G(d,p) level of theory. The calculations have been performed using the geometries optimized for this level of theory and using the TMS as reference.

The electronic properties, such as HOMO–LUMO energies, absorption wavelengths and oscillator strengths were calculated using B3LYP method of the time dependent TD-DFT based on the optimized structure in gas phase.

Results and discussion

Crystal structure

The compound 6-acetyl-2,2-dimethyl-chromane crystallizes in the triclinic P-1 space group with cell parameters a = 5.9622(5) Å,

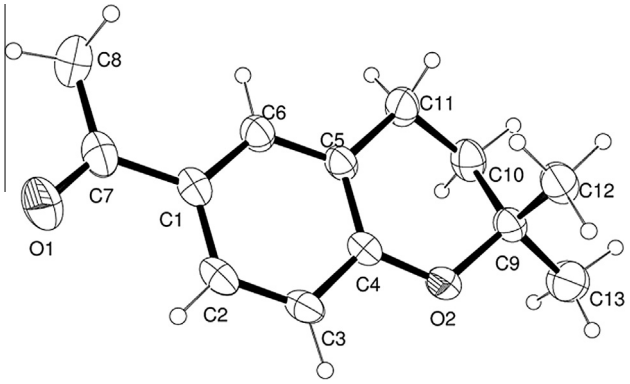

Fig. 1. View of the structure of 6-acetyl-2,2-dimethyl-chromane showing the labeling of non-H atoms and their displacement ellipsoids at the 30% probability level.

$b = 10.342(1)$ Å, $c = 10.464(1)$ Å, $\alpha = 63.81(1)°$, $\beta = 81.923(9)°$, $\gamma = 82.645(9)°$ and $Z = 2$ molecules per unit cell. Fig. 1 shows and ORTEP [26] plot of the chromane derivative molecule and their bond distances and angles are given in Table 2, observed intramolecular bond distances and angles conforms the organic chemistry rules. Particularly, the observed aromatic ring C—C bond distances are in the 1.372(2)–1.396(2) Å range as expected for a resonant bond structure. This delocalized π-bonding structure extends to the attached acetyl group and to the oxygen of the fused hetero-cycle ring hence stabilizing the planar conformation observed for the corresponding molecular fragment [*rms* deviation of non-H atoms from the best least-squares plane equal to 0.027 Å]. Single C—C bond distances in the chromane hetero-cycle are in the 1.506(2)–1.525(3) Å range.

Table 2
Selected experimental and calculated bond distances, angles and dihedral angles of 6-acetyl-2,2-dimethyl-chromane.

Parameters	Experimental[a]	Calculated[b]	
		B3LYP	mPW1PW91
C(1)—C(6)	1.391(2)	1.398	1.397
C(1)—C(2)	1.396(2)	1.406	1.400
C(1)—C(7)	1.488(2)	1.491	1.485
C(2)—C(3)	1.372(2)	1.381	1.376
C(3)—C(4)	1.400(2)	1.404	1.399
C(4)—O(2)	1.360(2)	1.359	1.351
C(4)—C(5)	1.396(2)	1.404	1.400
C(5)—C(6)	1.390(2)	1.395	1.391
C(5)—C(11)	1.506(2)	1.512	1.504
C(7)=O(1)	1.213(2)	1.219	1.214
C(7)—C(8)	1.495(3)	1.520	1.511
C(9)—O(2)	1.464(2)	1.461	1.446
C(9)—C(12)	1.506(2)	1.533	1.517
C(9)—C(13)	1.516(2)	1.526	1.525
C(9)—C(10)	1.519(2)	1.536	1.528
C(10)—C(11)	1.525(3)	1.531	1.521
C(1)—C(6)—C(2)	118.1(1)	118.3	118.4
C(6)—C(1)—C(7)	122.5(2)	122.9	122.9
C(2)—C(1)—C(7)	119.5(1)	118.8	118.7
C(3)—C(2)—C(1)	121.1(1)	120.7	120.6
C(2)—C(3)—C(4)	119.9(1)	120.2	120.2
O(2)—C(4)—C(5)	123.5(1)	123.5	123.4
O(2)—C(4)—C(3)	116.0(1)	116.1	116.1
C(5)—C(4)—C(3)	120.5(1)	120.5	120.5
C(6)—C(5)—C(4)	118.0(1)	118.1	118.1
C(6)—C(5)—C(11)	121.6(1)	121.9	121.8
C(4)—C(5)—C(11)	120.4(1)	120.0	120.1
C(1)—C(6)—C(5)	122.4(1)	122.3	122.2
O(1)—C(7)—C(1)	120.6(1)	120.9	120.9
O(1)—C(7)—C(8)	120.1(2)	120.1	120.3
C(1)—C(7)—C(8)	119.4(2)	118.9	118.8
O(2)—C(9)—C(12)	107.8(1)	108.0	108.1
O(2)—C(9)—C(13)	104.3(1)	104.4	104.6
C(12)—C(9)—C(13)	111.2(2)	110.9	110.9
O(2)—C(9)—C(10)	109.5(1)	109.1	109.1
C(12)—C(9)—C(10)	112.2(1)	112.7	112.5
C(13)—C(9)—C(10)	111.5(2)	111.2	111.1
C(9)—C(10)—C(11)	111.2(1)	111.8	111.4
C(5)—C(11)—C(10)	110.3(1)	110.6	110.4
C(4)—O(2)—C(9)	118.3(1)	119.5	118.9
Dihedral angles (°)			
C(6)—C(1)—C(2)—C(3)	1.1(2)	0.24	0.311
C(7)—C(1)—C(2)—C(3)	−178.9(1)	179.9	179.9
C(1)—C(2)—C(3)—C(4)	−0.2(2)	0.16	0.152
C(2)—C(3)—C(4)—O(2)	179.7(1)	−179.1	−179.1
C(2)—C(3)—C(4)—C(5)	−1.1(2)	−0.47	−0.57
O(2)—C(4)—C(5)—C(6)	−179.4(1)	178.8	178.9
C(3)—C(4)—C(5)—C(6)	1.4(2)	0.36	0.509
O(2)—C(4)—C(5)—C(11)	0.3(2)	−0.45	−0.11
C(3)—C(4)—C(5)—C(11)	−178.9(1)	−178.9	−178.5
C(2)—C(1)—C(6)—C(5)	−0.7(2)	−0.36	−0.37
C(7)—C(1)—C(6)—C(5)	179.3(1)	−179.9	−179.9
C(4)—C(5)—C(6)—C(1)	−0.5(2)	0.06	−0.03
C(11)—C(5)—C(6)—C(1)	179.8(2)	179.3	179.0
C(6)—C(1)—C(7)—O(1)	−175.9(2)	−179.9	−179.9
C(2)—C(1)—C(7)—O(1)	4.0(3)	0.43	0.42
C(6)—C(1)—C(7)—C(8)	2.8(3)	0.10	0.07
C(2)—C(1)—C(7)—C(8)	−177.2(2)	−179.5	−179.5
O(2)—C(9)—C(10)—C(11)	59.5(2)	57.6	59.04
C(12)—C(9)—C(10)—C(11)	−60.2(2)	−62.4	−61.02
C(13)—C(9)—C(10)—C(11)	174.4(2)	172.3	173.8
C(6)—C(5)—C(11)—C(10)	−162.0(2)	−160.5	−161.2
C(4)—C(5)—C(11)—C(10)	18.3(2)	18.7	17.8
C(9)—C(10)—C(11)—C(5)	−47.6(2)	−46.9	−46.6
C(5)—C(4)—O(2)—C(9)	11.8(2)	12.0	13.2
C(3)—C(4)—O(2)—C(9)	−168.9(1)	−169.4	−168.3
C(12)—C(9)—O(2)—C(4)	81.1(2)	82.9	80.8
C(13)—C(9)—O(2)—C(4)	−160.6(2)	−158.9	−160.8
C(10)—C(9)—O(2)—C(4)	−41.2(2)	−39.9	−41.9

[a] From structural X-ray diffraction methods.
[b] Computed with 6-311++G(d,p) basis set. See Fig. 1 for the atom numbering scheme.

Molecular structure

The potential energy surface scans for internal rotation around the C(8)C(7)C(1)C(6) dihedral angle (B3LYP/6-31G(d,p) level) were performed to evaluate the minima energy structures adopted by the title compound as shown in Fig. 2. Two different stable conformations were obtained according to the position of C=O group with respect to the C(1)=C(2) Bond (See Fig. 3). In conformer I (C_I), the C=O group is *syn* respect to the C=C bond and in conformer II (C_{II}), the carbonyl group is *anti* respect to the C=C bond. According to the crystal structure described previously, only C_I is observed in the solid. In C_{II}, the acetyl group is in the same plane as the molecular skeleton, moreover, in C_I, the C(8)C(7)C(1)C(6) dihedral angle is 0.10° indicating that the acetyl group is deviated above the molecular plane.

For both conformers identified above, the free energies calculated using the B3LYP/6-31G(d,p) level of theory were used, along with the average temperature of the experiment, to estimate (using the Boltzmann distribution) the amount of each conformer that should be observed in the gas phase. The difference in free energy was calculated to be 0.29 kJ mol^{-1}; therefore the ratio of C_I:C_{II} conformer was predicted to be 0.47:0.53. The difference in total energy calculated at the same level of theory is 1.10 kJ mol^{-1}. The dipolar

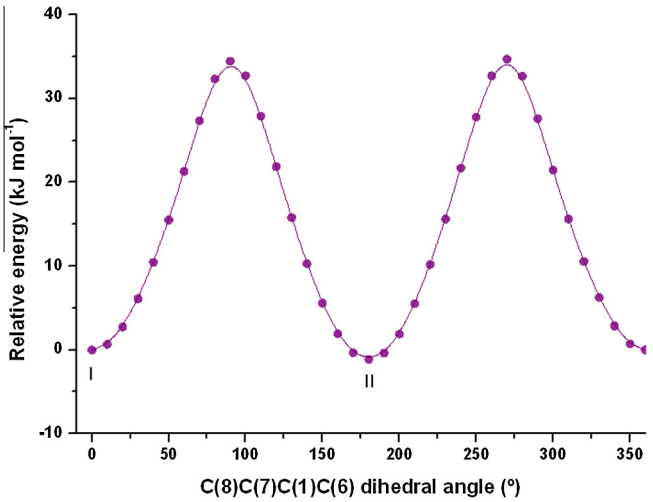

Fig. 2. Potential energy curve versus dihedral C(8)C(7)C(1)C(6) angle, calculated at B3LYP/6-31G(d,p) level of theory.

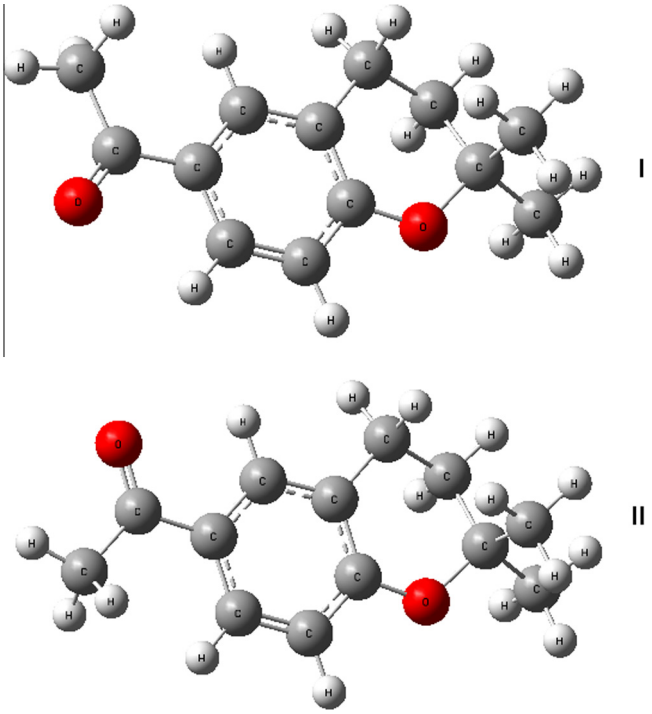

Fig. 3. Optimized molecular structure for both conformers of 6-acetyl-2,2-dimethyl-chromane calculated at B3LYP/6-311++G(d,p) level of theory.

moments of C_I and C_{II} conformers are 5.2418 and 3.5678 Debye, respectively. The high value of dipolar moment for the C_I conformer could explain its experimental stability, as observed by Sambrano et al for the M4 tautomer of 5-methylcytosine [27].

Table 2 shows a comparison of the calculated geometrical parameters of C_I conformer and the values determined experimentally by X-ray diffraction. The agreement between the optimized and experimental crystal structure is quite good showing that the geometry optimization almost exactly reproduces the experimental conformation.

NBO analysis

NBO analysis has been performed on the 6-acetyl-2,2-dimethyl-chromane compound at the B3LYP/6-311++G(d,p) level of theory to elucidate the intra-molecular, re-hybridization and delocalization of electron density within the molecule. natural bond orbital analysis provides an efficient method for studying intra- and inter-molecular bonding and interaction among bonds, and also provides a convenient basis for investigating charge transfer or conjugative interaction in molecular systems [28]. The larger E(2) value, the more intensive is the interaction between electron donors and electron acceptors, i.e., the more donating tendency from electron donors to electron acceptors and the greater the extent of conjugation of the whole system. Delocalization of electron density between occupied Lewis-type (bond or lone pair) NBO orbitals and formally unoccupied (anti-bond or Ryberg) non-Lewis NBO orbitals correspond to a stabilizing donor–acceptor interaction. The second-order Fock matrix was carried out to evaluate the donor–acceptor interactions in the NBO analysis [29]. The interactions result is a loss of occupancy from the localized NBO of the idealized Lewis structure into an empty non-Lewis orbital. For each donor (i) and acceptor (j), the stabilization energy E(2) associated with the delocalization $i \rightarrow j$ is estimated by:

$$E(2) = \Delta E_{ij} = q_i \frac{F(i,j)^2}{\varepsilon_j - \varepsilon_i}, \quad (1)$$

where q_i is the donor orbital occupancy, ε_i and ε_j are diagonal elements and F(i,j) is the off-diagonal NBO Fock matrix element.

The hyper-conjugative interactions are formed by the orbital overlap between π (C—C) bond orbital to π*(C—C) anti bonding orbital, which results in intra-molecular charge transfer causing the stabilization of the system. These interactions can be identified by finding the increase in electron density in the anti-bonding orbital. The strong intra-molecular hyper-conjugation interaction of the σ and π electrons of C—C to anti C—C and C—O bond in the ring leads to stabilization of some part of the ring as evident from Table 3. A very strong interaction has been observed between the p-type orbital containing the lone electron pair of O(2) and the neighbor π^* C(4)—C(5) anti-bonding orbital of the benzene ring. The lone pair LP O(1) in both conformers participates in interactions LP O(1) → σ^* C(1)—C(7) and LP O(1) → σ^* C(7)—C(8). As shown in Table 3, the hyper-conjugative effect is higher in C_I compared with C_{II}. The interaction π^* C(4)—C(5) → π^* C(2)—C(3) produces a great stabilization of 254.03 kJ mol^{-1} in C_I conformer whereas in C_{II} it is absent.

The relation between the electron occupation of the σ^* C(7)—C(8) orbital and the bond lengths C(7)—C(8) and C(7)═O(1) has been investigated in both conformers. Table S4 shows the C—C and C═O bond lengths with the corresponding electron occupancy of the natural bond orbitals of both conformers of the title compound. As shown in Table S4, the C—C bond length in C_I is

Table 3
Second-order perturbation theory analysis of the Fock matrix for the two conformers of 6-acetyl-2,2-dimethyl-chromane by the NBO method.

Interaction (donor → acceptor)[a]	E(2) in kJ mol^{-1}[b]	
	C_I	C_{II}
π C(1)—C(6) → π* C(5)—C(4)	17.29	18.01
π C(1)—C(6) → π* C(2)—C(3)	20.35	22.95
π C(1)—C(6) → π* C(7)═O(1)	19.88	19.82
π C(4)—C(5) → π* C(1)—C(6)	24.18	25.12
π C(4)—C(5) → π* C(2)—C(3)	14.82	16.17
π C(2)—C(3) → π* C(5)—C(4)	22.31	21.42
π C(2)—C(3) → π* C(1)—C(6)	16.40	15.95
LP O(2) → π* C(4)—C(5)	29.57	29.32
LP O(1) → σ* C(1)—C(7)	20.29	20.26
LP O(1) → σ* C(7)—C(8)	21.52	21.49
π* C(4)—C(5) → π* C(2)—C(3)	254.03	–

[a] See Fig. 1 for atoms numbering scheme.
[b] E(2) means energy of hyper-conjugative interactions.

slightly longer than that of C_{II}, which is in agreement with the high occupancy of the σ^* C(7)—C(8) in C_I. This result accords with the higher LP O(2) → σ^* C(7)—C(8) energy interaction in C_I which produces a lengthening of the C—C bond and a shortening of the C═O bond as compared with C_{II} conformer.

NMR analysis

Following geometry optimization of 6-acetyl-2,2-dimethylchromane, Gauge-Including Atomic Orbital (GIAO) method was used to predict ^{1}H NMR chemical shifts using DFT-B3LYP functional with 6-311++G(d,p) basis sets.

The relationship between the experimental ^{1}H chemical shifts (δ_{exp}) and (GIAO) magnetic isotropic shielding constants (δ_{calc}) is usually linear and described by the following equation: $\delta_{exp} = a + b\,\delta_{calc}$ [30–32]. The slope and intercept of the least-squares correlation are utilized to predict chemical shifts, and the linear correlation coefficient (R) is used to verify the precision and the agreement between experimental and theoretical data. Fig. 4 shows the linear regression between the experimental and theoretical ^{1}H NMR chemical shifts. In the present study, the correlation coefficient for proton chemical shift is determined as 0.98848. This proves fair agreement between the experimental and their calculated data. According to the comparison between calculated data and experimental counterparts, the calculated chemical shifts are in acceptable agreement with the experimental results. Table 4 shows the calculated and experimental chemical shifts with the corresponding tentative assignment. The experimental ^{1}H NMR spectrum is shown in Fig. S2. The aromatic protons H-9, H-3 and H-8 appear at δ 7.74, 7.72 and 6.80 ppm as *d* (J = 2.2 Hz), dd (J = 8.9 and 2.2 Hz) and broad *d* (J = 8.9), respectively. The triplets (2H each) at δ 2.82 and 1.83 ppm are assigned to the 13-CH_2 and 16-CH_2 of the pyrane ring, respectively (see Fig. S3 for atoms numbering). The singlet of 3H at δ 2.53 ppm is assigned to the protons of the acetyl group while the singlet of 6H at δ 1.36 ppm is assigned to the protons of the *gem*-dimethyl group linked to the pyrane ring.

Vibrational study

The 6-acetyl-2,2-dimethyl-chromane molecule lacks of any symmetry (C_1 point group). Therefore, all 87 normal modes of vibrations are both IR- and Raman-active. The assignment of modes to observed bands in the solid state FTIR and Raman spectra of the compound was assisted by the theoretically predicted frequencies for the modes. These were calculated in the harmonic approximation at the B3LYP/6-31G(d,p) level of theory. The experimental IR and Raman spectra are shown in Fig. 5 whereas the simulated IR and Raman spectra for the C_I conformer are presented in Fig. S4. The experimental and calculated vibration frequencies are compared in Table 5 along a tentative mode assignment. It is to be noted some discrepancy between observed and calculated frequencies that can in part be due to the fact that the inter-molecular interactions unavoidably present in the solid state is not taken into account in the gas phase theoretical calculations. Vibration mode frequencies calculated at B3LYP/6-31G(d,p) level of theory were scaled by 0.9608 to correct for theoretical error in this work [33].

Table 4
Experimental and calculated ^{1}H NMR chemical shifts (ppm).

Atom[a]	Calculated[b]	Experimental[c]
H9	8.32	7.74 d
H3	7.68	7.72 dd
H8	6.98	6.80 d
H15	2.96	2.82 t
H14	2.73	
H30	2.58	2.53 s
H29	2.57	
H31	2.01	
H18	1.78	1.83 t
H17	1.76	
H26	1.69	1.36 s
H23	1.61	
H27	1.37	
H21	1.28	
H25	1.19	
H22	0.88	

[a] See Fig. S3 for the atom numbering scheme.
[b] Calculated at B3LYP/6-311++G(d,p) level of theory.
[c] NMR spectrum measured in $CDCl_3$.

CH_3 vibrations

The anti-symmetric and symmetric stretching modes of the methyl group normally appear at about 3100 and 2880 cm^{-1}. The bands observed at 3051 and 3013 cm^{-1} in the IR spectrum and at

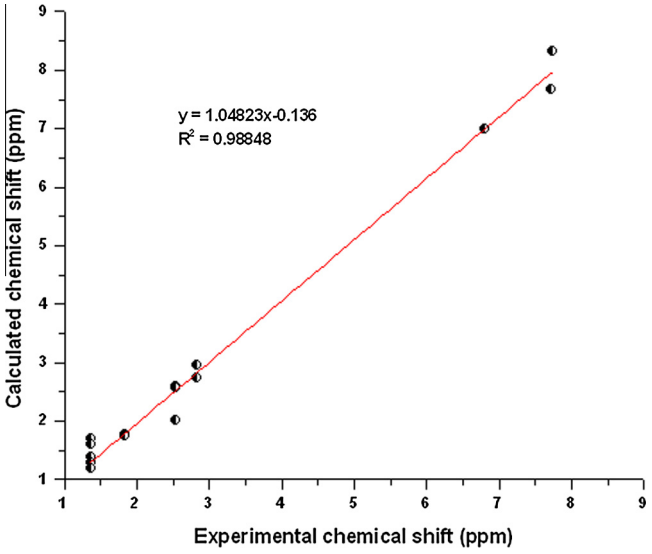

Fig. 4. Correlation between experimental and calculated ^{1}H NMR chemical shifts. Calculations performed at the B3LYP/6-311++G(d,p) level.

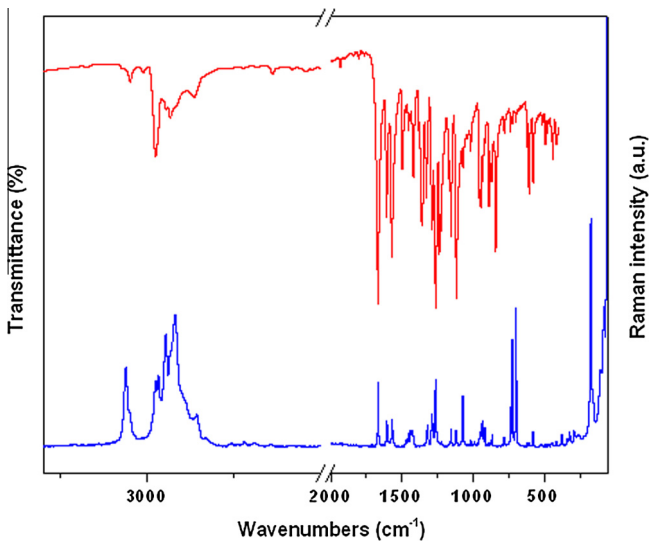

Fig. 5. Solid state IR transmission (upper trace) and Raman dispersion spectra (lower trace) of 6-acetyl-2,2-dimethyl-chromane.

Table 5
Observed and calculated mode frequencies (in cm^{-1}) and tentative assignments for 6-acetyl-2,2-dimethyl-chromane vibrations.

Mode	Experimental		Calculated[c]		Tentative assignment[d,e]
	IR[a]	Raman[b]	Unscaled	Scaled	
1	–	–	3229 (4)	3102	ν C(4)—H
2	3068 sh	–	3210 (11)	3084	ν C(3)—H
3	–	3063 (34)	3188 (4)	3063	ν C(6)—H
4	3051 w	3053 (15)	3168 (29)	3044	ν_a CH_3
5	–	–	3139 (9)	3016	ν_a CH_3
6	3013 vw	–	3136 (17)	3013	ν_a CH_3
7	–	–	3134 (9)	3011	ν_a CH_3
8	–	–	3127 (6)	3004	ν_a CH_3
9	2978 m	2977 (28)	3111 (60)	2989	ν_a CH_3CO
10	2970 sh	2969 (30)	3097 (29)	2976	ν_a $C(10)H_2$
11	2947 vw	2948 (48)	3065 (28)	2945	ν_a $C(11)H_2$
12	–	–	3063 (16)	2943	ν_s CH_3
13	2935 w	2934 (41)	3057 (24)	2937	ν_s CH_3
14	–	–	3052 (3)	2932	ν_s CH_3CO
15	2919 sh	2920 (57)	3051 (22)	2931	ν_s $C(10)H_2$
16	–	2858 (13)	3030 (10)	2911	ν_s $C(11)H_2$
17	1669 vs	1668 (28)	1768 (200)	1699	ν C=O
18	1608 s	1606 (11)	1664 (118)	1598	ν C(1)—C(6) + ν C(3)—C(4)
19	1572 s	1570 (11)	1622 (121)	1558	ν C(4)—C(5) + ν C(1)—C(2)
20	1499 m	–	1547 (37)	1486	δ_a $C(13)H_3$ + δ $C(11)H_2$
21	1474 vw	1473 (2)	1540 (25)	1480	δ_a $C(12)H_3$
22	1456 w	1457 (5)	1526 (10)	1466	δ_a $C(12)H_3$
23	1454 w	–	1524 (12)	1464	δ_a $C(12)H_3$ + δ $C(10)H_2$
24	–	1440 (7)	1519 (3)	1459	δ $C(10)H_2$
25	–	1431 (7)	1509 (1)	1450	δ $C(11)H_2$
26	–	–	1508 (8)	1449	δ_a $C(8)H_3$
27	–	–	1502 (<1)	1443	δ $C(10)H_2$ + δ_a $C(8)H_3$
28	1420 m	1420 (4)	1500 (45)	1441	δ_a $C(8)H_3$
29	–	–	1465 (11)	1408	ν C(5)—C(6) + ν C(1)—C(6) + δ C(6)—H
30	–	–	1448 (8)	1391	δ_s $C(13)H_3$
31	1381 w	–	1430 (15)	1374	δ_s $C(12)H_3$
32	1365 s	–	1408 (65)	1353	δ_s $C(8)H_3$
33	1358 s	–	1397 (55)	1342	ω $C(10)H_2$ + τω $C(11)H_2$
34	1330 m	1327 (6)	1375 (39)	1321	ω $C(11)H_2$ + τω $C(10)H_2$
35	1321 w	1320 (9)	1370 (15)	1316	ν C(4)—C(5) + ν C(3)—C(4) + ν C(1)—C(6)
36	1289 m	1290 (14)	1324 (92)	1272	δ C(6)—H + δ C(3)—H + δ C(2)—H
37	1264 s	1265 (6)	1305 (281)	1254	ν C(4)—O(2) + ν C(1)—C(7)
38	–	1256 sh	1301 (3)	1250	ν C(1)—C(7)
39	1238 m	1239 (2)	1293 (63)	1242	ν C(9)—O(2) + ρ $C(10)H_2$
40	1227 m	1224 (2)	1274 (61)	1224	τω $C(11)H_2$
41	1172 w	–	1260 (30)	1210	τω $C(10)H_2$
42	1156 m	1155 (7)	1198 (106)	1151	δ C(3)—H + δ C(2)—H
43	1123 sh	1121 (6)	1189 (45)	1142	ρ $C(12)H_3$ + τω $C(11)H_2$
44	1116 m	1117 sh	1158 (68)	1113	ρ $C(13)H_3$ + τω $C(10)H_2$
45	–	1093 (1)	1147 (5)	1102	δ C(2)—H + δ C(3)—H
46	1072 w	1073 (22)	1102 (60)	1059	ρ $C(8)H_3$ + δ C(2)—H + δ C(6)—H
47	1018 vw	1016 (2)	1063 (5)	1021	ρ $C(11)H_2$ + ρ $C(13)H_3$ + ρ $C(12)H_3$
48	–	–	1055 (<1)	1014	ρ $C(8)H_3$
49	991 vvw	991 (2)	1033 (2)	993	ν C(10)—C(11) + ρ $C(13)H_3$
50	–	967 (1)	1017 (1)	977	ρ $C(13)H_3$ + ρ $C(8)H_3$ + ρ $C(10)H_2$
51	956 w	954 sh	988 (64)	949	γ C(3)—H + γ C(2)—H
52	947 w	945 (10)	972 (58)	934	ρ $C(11)H_2$ + δ C(2)C(1)C(6) + γ C(3)—H
53	933 vw	933 (10)	968 (24)	930	ν C(7)—C(8) + δ C(2)—H + δ C(3)—H
54	919 vw	919 (8)	951 (11)	914	δ C(1)C(6)C(5) + ν C(9)—C(12) + ν C(9)—C(13)
55	889 w	889 (1)	931 (16)	895	δ C(1)C(2)C(3) + ν C(9)—C(10) + γ C(6)—H + ν C(9)—C(12)
56	876 vw	876 (1)	911 (3)	875	γ C(6)—H
57	870 vw	869 (6)	901 (5)	866	γ C(6)—H + ν C(9)—O(2) + δ C(5)C(11)C(10)
58	–	–	883 (5)	848	δ C(1)C(2)C(3) + ρ $C(10)H_2$
59	843 m	–	857 (56)	823	γ C(2)—H + γ C(2)—H
60	781 vw	782 (3)	790 (6)	759	δ C(4)C(5)C(6) + δ C(4)O(2)C(9)
61	738 vvw	739 (17)	745 (5)	716	γ C(5)C(4)C(3) + γ C(6)—H + γ C(3)—H
62	724 vvw	725 (46)	732 (5)	703	γ C(6)C(5)C(4) + γ C(2)C(1)C(6) + ρ $C(11)H_2$
63	700 vvw	699 (60)	710 (7)	682	δ C(2)C(3)C(4) + ρ $C(11)H_2$ + ρ $C(10)H_2$
64	623 w	622 (1)	634 (4)	609	ρ $C(8)H_3$ + γ C(2)C(1)C(6) + γ C(3)—H
65	608 m	608 (2)	617 (36)	593	δ C=O + δ C(3)—H
66	580 m	580 (6)	590 (18)	567	δ C(5)C(11)C(10) + δ C(1)C(6)C(5) + δ C(2)C(3)C(4)
67	514 vw	–	529 (6)	508	γ C=O + γ C(1)C(2)C(3) + γ C(6)—H
68	494 w	493 (1)	519 (9)	499	δ C(13)C(9)C(12) + δ C(9)O(2)C(4) + δ C(6)—H
69	479 vw	476 (1)	498 (3)	478	δ C(9)C(10)C(11) + δ C(9)O(2)C(4)
70	451 sh	452 (2)	481 (2)	462	δ C(8)C(7)C(1) + δ C(3)—H + δ C(10)C(9)C(12)
71	442 w	442 (2)	454 (2)	436	γ C(6)C(5)C(4) + γ C(3)—H
72	416 w	416 (2)	453 (4)	435	δ C(10)C(9)O(2) + τ CCCC
73	–	378 (5)	410 (2)	394	δ C(10)C(9)C(12) + δ C(8)C(7)C(1)

Table 5 (*continued*)

Mode	Experimental		Calculated[c]		Tentative assignment[d,e]
	IR[a]	Raman[b]	Unscaled	Scaled	
74	–	350 (1)	378 (3)	363	δ O(12)C(11)C(28) + τ CCCC + δ C(12)C(9)C(13)
75	–	338 (3)	336 (2)	323	τ CCCC
76	–	322 (6)	320 (1)	307	τ COCC + τ CCCC
77	–	291 (7)	286 (2)	275	τ $C(13)H_3$ + τ CCCC
78	–	264 (5)	271 (<1)	260	τ $C(12)H_3$ + τ $C(13)H_3$
79	–	249 (4)	258 (<1)	248	τ CCCC + τ C(11)—C(5)
80	–	–	239 (1)	229	τ $C(13)H_3$ + τ $C(12)H_3$
81	–	–	211 (<1)	202	τ CCCC + τ $C(12)H_3$ + τ $C(13)H_3$
82	–	173 (100)	157 (1)	151	τ CCCC + τ $C(8)H_3$
83	–	156 (20)	154 (<1)	148	τ $C(8)H_3$
84	–	–	140 (1)	135	τ CCCC
85	–	105 (35)	113 (2)	109	γ C(9)O(2)C(4) + τ CCCC
86	–	82 (60)	58 (2)	55	τ C(7)C(1)
87	–	–	45 (<1)	43	τ ring

[a] sh, shoulder; s, strong; w, weak; m, medium; v, very.
[b] Relative band heights in parentheses.
[c] Calculated at B3LYP/6-31G(d,p) level of theory. IR intensities in parenthesis.
[d] ν: stretching, δ: in-plane deformation, γ: out-of-plane deformation, ρ: rocking, ω: wagging, τω: twisting, τ: torsion modes.
[e] See Fig. 1 for the atoms numbering scheme.

3052 cm^{-1} in Raman are assigned to the anti-symmetric stretching vibration of the methyl groups linked to the pyrane ring. The medium intensity IR band located at 2978 cm^{-1} (2977 cm^{-1} in Raman) is assigned to the anti-symmetric mode of the acetyl methyl group. The weak IR band observed at 2935 cm^{-1} is assigned to the methyl symmetric stretching vibration.

The anti-symmetric methyl deformation modes are observed at 1499, 1474, 1456, 1454 and 1420 cm^{-1} in the IR spectrum and at 1473, 1457, and 1420 cm^{-1} in Raman. The IR bands at 1381 and 1365 cm^{-1} are assigned to the symmetrical methyl deformation mode. The IR bands located at 1123, 1116, 1072, 1018 cm^{-1} are assigned to the rocking mode.

CH_2 vibrations

The IR bands at 2970 and 2947 cm^{-1} (2969 and 2948 cm^{-1} in Raman) are assigned to the anti-symmetric stretching mode. The Raman dispersions due to the symmetric stretching vibrations appear as an intense band at 2920 cm^{-1} and a weak band at 2858 cm^{-1} and the counterpart IR bands for these modes are appear at 2919 and 2864 cm^{-1}. The Raman bands corresponding to the methylene bending modes are observed at 1440 and 1431 cm^{-1}. The modes corresponding to the wagging, twisting and rocking of methylene group are all assigned and given in Table 5.

CH vibrations

The aromatic compounds show C—H vibration modes in the 3300–3100 cm^{-1} region. The bands observed at 3068 cm^{-1} (IR) and at 3063 cm^{-1} (Raman) are assigned to the previously mentioned mode. In aromatic compounds the C—H in-plane bending vibrations are observed in the region from 1300 to 850 cm^{-1} and are usually weak. The bands due to the C—H in-plane ring vibration coupled with C—C stretching vibration are observed as a number of sharp medium to weak intensity bands in the 1300–1000 cm^{-1} spectral region. In the present study, the IR bands at 1289, 1156 and 1072 cm^{-1} and the Raman bands at 1290, 1155, 1093 and 1073 cm^{-1} are assigned to the C—H in-plane bending vibrations as reported in Table 5. The C—H out-of-plane bending vibrations are strongly coupled vibrations and occur in the region from 950 to 600 cm^{-1} [2,30–36]. The IR bands observed at 956, 947, 933, 876, 870, 843 and 738 cm^{-1} and the Raman bands at 954, 945, 933, 876, 869 and 739 cm^{-1} confirm the presence of C—H out-of-plane bending vibrations, hence agreeing with the values reported in literature [2,30–36].

C-C and ring vibrations

The phenyl group C—C stretching mode frequencies are expected in the spectral range from 1650 to 1200 cm^{-1}. The actual frequencies of these modes are determined not only by the nature of the substituents themselves but mainly by the way these are linked around the ring. The ring C—C stretching bands appear in the IR spectrum at 1608, 1572 and 1321 cm^{-1} and at 1606, 1570 and 1320 cm^{-1} in Raman. The observed and calculated C—C—C in-plane and out-of-plane bending modes are presented in Table 5 along with their assignment. These results are in good agreement with corresponding literature data and provide support to values derived from theoretical calculations [2,30–36].

C=O vibrations

The C=O stretching mode is observed in the IR spectrum as a very strong band at 1669 cm^{-1} and in Raman as a weak band at 1668 cm^{-1}. This mode is observed at 1666 cm^{-1} in the IR spectrum of 4-hydroxy-3-(3-methyl-2-butenyl)acetophenone [2] hence indicating that the acetylketo stretching vibration is not all influenced by the ring substituents. The spectral features and assignment of the C=O in-plane and out-of-plane bending vibrations are included in Table 5.

Frontier molecular orbitals

The conjugated molecules are characterized by a HOMO–LUMO separation which is the result of a significant degree of intermolecular charge transfer from the end-capping electron-donor to the efficient electron acceptor group through a π-conjugated path. The strong charge-transfer interaction through a π-conjugated bridge results in substantial ground state donor–acceptor mixing and the appearance of charge-transfer band in the electronic absorption spectrum. Therefore, an electron density transfer occurs from the most aromatic part of the π-conjugated system in the electron-donor side to the electron-withdrawing part [37]. A deeper understanding of chemical reactivity can be gained by this electron absorption which corresponds to the transition from the ground to the first excited state and it is mainly described by one-electron excitation from the HOMO to the LUMO orbital.

Molecular orbitals, when viewed in a qualitative graphical representation, can provide insight into the nature of reactivity, and also into some of the structural and physical properties of molecules. Well-known concepts such as conjugation, aromaticity and lone pairs are well illustrated by molecular orbitals. Molecular orbital coefficients analysis showed that the frontier molecular orbital (FMOs) are composed mainly of π-atomic orbitals. Hence, the electronic spectrum corresponding to electronic transitions are mainly of $\pi \rightarrow \pi^*$ nature.

The energy levels of the HOMO, LUMO, HOMO-1, HOMO-2 and LUMO + 1 orbitals computed at the B3LYP/6-31G(d,p) level of theory for 6-acetyl-2,2-dimethyl-chromane are represented in Fig. 6(a). As can be appreciated in the figure, the HOMO is localized on the benzene ring, O—C=O part, the methylene group of the pyrane ring, and the O atom of the hetero-atomic ring. The LUMO is characterized by a charge distribution on the benzene ring, the acetyl group, and the O located in the pyrane ring.

The HOMO–LUMO energy gap is a relevant value which serves as a stability index. In fact, a large HOMO–LUMO gap implies high molecular stability in the sense of its lower reactivity in chemical reactions [37,38,32,39]. The energy values of HOMO and LUMO molecular orbitals with the corresponding HOMO–LUMO energy gap is shown in Fig. 6(b). The LUMO as an electron acceptor represents the ability to obtain an electron, and HOMO represents the ability to donate an electron. The energy gap value of HOMO–LUMO (3.54 eV) explains the eventual charge transfer interaction within the molecule, which influences the biological activity of the molecule. Consequently, the lowering of the HOMO–LUMO band gap is essentially a consequence of the large stabilization of the LUMO due to the strong ability of the electron-acceptor group.

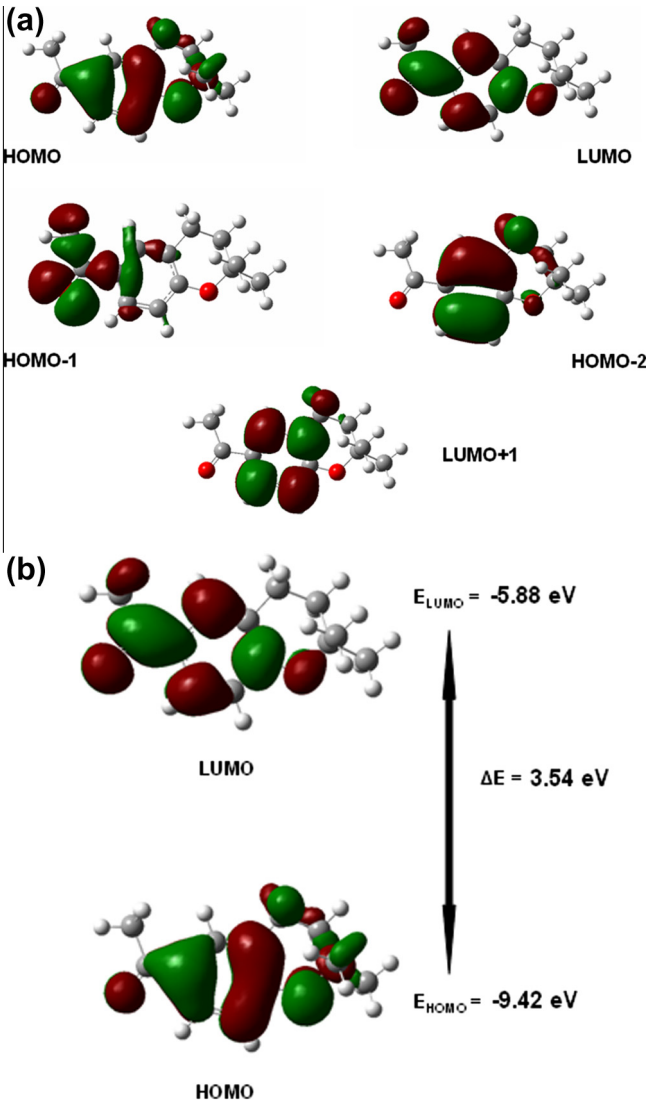

Fig. 6. (a) Molecular orbitals involved in the electronic transitions of 6-acetyl-2,2-dimethyl-chromane and (b) atomic orbital composition of the frontier molecular orbital for 6-acetyl-2,2-dimethyl-chromane.

UV–Visible spectra analysis

To understand the nature of electronic transitions within 6-acetyl-2,2-dimethyl-chromane molecule, TD-DFT calculations on electronic absorption spectra in gas phase were performed. The λ_{max} values are obtained from the UV–Visible spectra analyzed theoretically with B3LYP/6-31G(d,p) level of theory. The calculated UV absorption maxima (which are a function of electron availability), theoretical electronic excitation energies, and oscillator strengths are detailed in Table 6. The experimental and theoretically predicted UV–Visible spectra are visualized in Fig. 7. As can be seen from Table 6, the calculated absorption maxima values for 6-acetyl-2,2-dimethyl-chromane have been found to be 323, 267 and 259 nm. The oscillator strength for the transition at 267 nm is higher in magnitude compared to other transitions and its corresponding experimental value is observed at 281 nm. The maximum absorption at 281 nm is assigned to the transition from

Table 6
Theoretical electronic absorption spectra of 6-acetyl-2,2-dimethyl-chromane calculated at B3LYP/6-311++G(d,p) level of theory.

Excited state	Wavelength (nm)		Excitation energies (eV)	Oscillator strengths (*f*)	Assignment[a]
	Experimental	Theoretical			
S1	–	323	3.8445	0.0001	H-1 → L
S2	281	267	4.6423	0.2960	H → L
S3	227	259	4.7789	0.0755	H-2 → L H → L + 1

[a] H = highest occupied molecular orbital; L = lowest unoccupied molecular orbital.

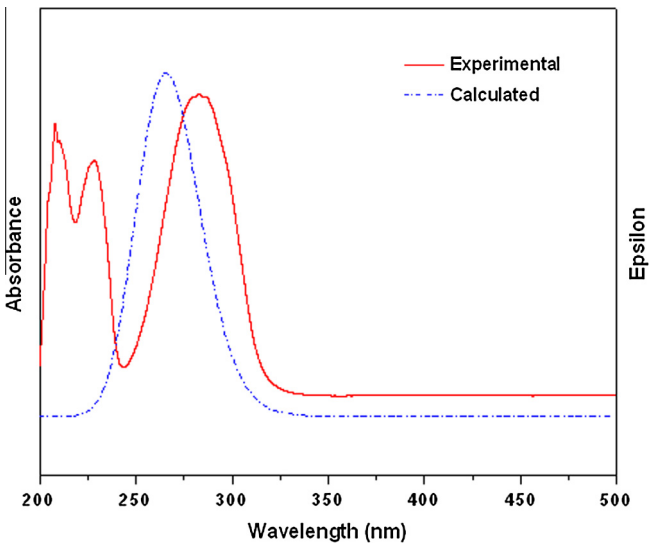

Fig. 7. Experimental and calculated UV–Visible absorption spectra of 6-acetyl-2,2-dimethyl-chromane.

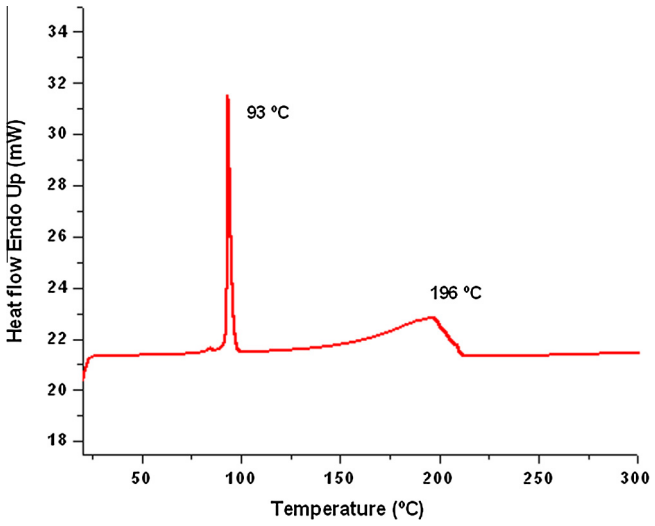

Fig. 8. DSC curve for solid state 6-acetyl-2,2-dimethyl-chromane.

HOMO orbital to LUMO one. This transition (H → L) is predicted to be of $\pi \rightarrow \pi^*$ nature (see Fig. 6(b)).

The absorption band at 323 nm in the calculated spectrum is assigned to HOMO-1 → LUMO transition. This band was not observed experimentally probably because it is obliterated by the much more intense absorption band at 281 nm. The observed band at 227 nm is mainly generated by excitations from HOMO-2 → LUMO and HOMO → LUMO + 1 (calculated wavelength of 259 nm). Ultraviolet radiation having wavelengths near or less than 200 nm is difficult to handle, and is seldom used as a routine tool for structural analysis.

Differential Scanning Calorimetry (DSC) study

The aim of the present DSC study was to examine the possible structural transitions and evaluate the thermodynamic parameters associated to the melting point of the compound. Fig. 8 shows the DSC curve for 6-acetyl-2,2-dimethyl-chromane in solid state. The DSC scan clearly shows an endothermic transition at 93 °C. This transition is attributed to the melting of the sample. The value agrees reasonably well with that obtained experimentally using an Ernest Leite microscope (94–95 °C). The estimated ΔH and ΔS variations for the phase transition are 22.1 kJ mol^{-1} and 60.36 J mol^{-1} K^{-1}, respectively. The endothermic peak located at 196 °C can be attributed to the decomposition of the substance.

4. Conclusions

The 6-acetyl-2,2-dimethyl-chromane compound was synthesized for the first time by using 4-hydroxi-3-(3-methyl-2-butenyl)-acetophenone as precursor. The substance was fully characterized by MS spectrometry, ^{1}H NMR, UV–Visible, IR and Raman spectroscopy and also by single crystal structural X-ray diffraction methods. The solid state molecular fragment is planar due to extended π-bonding delocalization. This arrangement is similar to that predicted by quantum chemical calculations. IR and Raman, ^{1}H NMR and UV–Vis spectra of the title compound was recorded and simulated by DFT approaches. The TD-DFT calculation assisted the assignment of electronic transitions observed in the UV–Vis absorption spectrum. The HOMO–LUMO energy gap is calculated to be 3.54 eV wide. The computed ^{1}H NMR chemical shift values compare well with the experimental values. DSC measurements show that the substance melts at 93 °C and decomposes at temperatures higher than 196 °C.

Acknowledgments

D.M.G. and A.B.A. thank CIUNT (Project 26D-411) and CONICET (PIP 0629) for financial support. C.A.N.C and E.L. thank CIUNT (Project 26D-416) and CONICET (PIP 0225) for financial support. E.L. and D.M.G. thank CONICET for postdoctoral fellowships. This work was supported by CONICET (PIP 1529), and by ANPCyT (PME06 2804 and PICT06 2315) of Argentina (O.E.P. and G.A.E.). Authors thank Mr. Marcelo Arias for Raman and DSC measurements.

Appendix A. Supplementary material

Tables of fractional coordinates and equivalent isotropic displacement parameters of the non-H atoms (Table S1), atomic anisotropic displacement parameters (Table S2), and hydrogen atoms positions (Table S3). Supplementary data associated with this article can be found, in the online version, at http://dx.doi.org/10.1016/j.saa.2014.02.035.

References

[1] G.P. Ellis, Chromenes, Chromanones, and Chromones (In Chemistry of Heterocyclic Compounds), Wiley, New York, 1977. 11–141.
[2] E. Lizárraga, E. Romano, R.A. Rudyk, C.A.N. Catalán, S.A. Brandán, Spectrochim. Acta Part A 97 (2012) 202.
[3] P. Proksch, E. Rodriguez, Phytochemistry 22 (1983) 2335.
[4] R.S. Bowers, T. Ohta, J.S. Cleere, P. Marsella, Science 193 (1976) 542.
[5] A.R. Katrikzy, C.W. Rees, E.F.V. Scriven, A. McKillop, A Comprehensive Heterocyclic Chemistry II, Elsevier, Amsterdam, 1996.
[6] M. Kidwai, S. Saxena, M.K.R. Khan, S.S. Thukral, Bioorg. Med. Chem. Lett. 15 (2005) 4295.
[7] M.M. Khafagy, A.H.F. Abd El-Wahab, F.A. Eid, A.M. El-Agrody, IL Farmaco 57 (2002) 715.
[8] J.H.G. Lago, C.S. Ramos, D.C.C. Casanova, A.D. Morandim, D.C.B. Bergamo, A.J. Cavalheiro, V.S. Bolzani, M. Furlan, E.F. Guimaraes, M.C.M. Young, M.J.J. Kato, J. Nat. Prod. 67 (2004) 1783.
[9] J. da Silva Mota, A.C. Leite, J.M. Batista, S.N. López, D.L. Ambrósio, D. Duó Passerini, M.J. Kato, V. da Silva Bolzani, R.M. Barretto Cicarelli, M. Furlan, Planta Med. 75 (2009) 620.
[10] W. Kemnitzer, S. Kasibhatla, S.C. Jiang, H. Zhang, J.H. Zhao, S.J. Jia, L.F. Xu, C. Crogan-Grundy, R. Denis, N. Barriault, L. Vaillancourt, S. Charron, J. Dodd, G. Attardo, D. Labrecque, S. Lamothe, H. Gourdeau, B. Tseng, J. Drewe, S.X. Cai, Bioorg. Med. Chem. 15 (2005) 4745.
[11] A. Afantitis, G. Melagraki, H. Sarimveis, P.A. Koutentis, J. Markopoulos, O. Igglessi-Markopoulou, Bioorg. Med. Chem. 14 (2006) 6686.
[12] T.A. Engler, K.O. LaTessa, R. Iyengar, W.Y. Chai, K. Agrios, Bioorg. Med. Chem. 4 (1996) 1755.
[13] Y. Kashiwada, K. Yamazaki, Y. Ikeshiro, T. Yamagishi, T. Fujioka, K. Mihashi, K Mizuki, L.M. Cosentino, K. Fowke, S.L. Morris-Natschke, K.H. Lee, Tetrahedron 57 (2001) 1559.
[14] R.F. Kaltenbach, S.P. Robinson, G.L. Trainor, PCTU.S. Pat. 20,050,267,183, 2005.
[15] X. Zhang, Z. Sui, Z. PCT U.S. Pat. 20,060,020,018, 2006.
[16] E.D. Glendening, J.K. Badenhoop, A.D. Reed, J.E. Carpenter, F.F. Weinhold, Theoretical Chemistry Institute, University of Wisconsin, Madison, WI, 1996.
[17] M.J.A. Marchese, C.S. de Heluani, C.A.N. Catalán, C.A. Griffin, J.B. Vaughn, W. Herz, Biochem. System. Ecol. 35 (2007) 169.
[18] F. Bohlmann, M. Grenz, Chemische Berichte 103 (1970) 90.
[19] F. Tomás-Barberán, E. Iniesta-San Martín, F. Tomás-Lorente, A. Rumbero, Phytochemistry 29 (1990) 1093.
[20] M.A. Ponce, E. Gros, An. Asoc. Quim. Argent. 79 (5) (1991) 197.
[21] CrysAlisPro, Oxford Diffraction Ltd., version 1.171.33.48 (release 15.09.2009 CrysAlis171.NET).
[22] G.M. Sheldrick, SHELXS-97. Program for Crystal Structure Resolution, Univ. of Göttingen, Göttingen, Germany, 1997;
G.M. Sheldrick, Acta Crystallogr. A 46 (1990) 467–473.
[23] G.M Sheldrick, SHELXL-97. Program for Crystal Structures Analysis, Univ. of Göttingen, Göttingen, Germany, 1997;
G.M. Sheldrick, Acta Crystallogr. A 64 (2008) 112–122.
[24] M.J. Frisch, J.A. Pople, J.S. Binkley, J. Chem. Phys. 80 (1984) 3265;
M.J. Frisch, G.W. Trucks, H.B. Schlegel, G.E. Scuseria, M.A. Robb, J.R. Cheeseman, J.A. Montgomery Jr., T. Vreven, K.N. Kudin, J.C. Burant, J.M. Millam, S.S. Iyengar, J. Tomasi, V. Barone, B. Mennucci, M. Cossi, G. Scalmani, N. Rega, G.A. Petersson, H. Nakatsuji, M. Hada, M. Ehara, K. Toyota, R. Fukuda, J. Hasegawa, M. Ishida, T. Nakajima, Y. Honda, O. Kitao, H. Nakai, M. Klene, X. Li, J.E. Knox, H.P. Hratchian, J.B. Cross, C. Adamo, J. Jaramillo, R. Gomperts, R.E. Stratmann, O. Yazyev, A.J. Austin, R. Cammi, C. Pomelli, J.W. Ochterski, P.Y. Ayala, K. Morokuma, G.A. Voth, P. Salvador, J.J. Dannenberg, V.G. Zakrzewski, S. Dapprich, A.D. Daniels, M.C. Strain, O. Farkas, D.K. Malick, A.D. Rabuck, K. Raghavachari, J.B. Foresman, J.V. Ortiz, Q. Cui, A.G. Baboul, S. Clifford, J.

Cioslowski, B.B. Stefanov, G. Liu, A. Liashenko, P. Piskorz, I. Komaromi, R.L. Martin, D.J. Fox, T. Keith, M.A. Al-Laham, C.Y. Peng, A. Nanayakkara, M. Challacombe, P.M.W. Gill, B. Johnson, W. Chen, M.W. Wong, C. González, J.A. Pople, Gaussian 03, revision C.02, Gaussian Inc, Wallingford, CT, 2004.
[25] R. Ditchfield, Mol. Phys. 8 (1974) 397.
[26] C.K. Johnson, ORTEP-II. A Fortran thermal-ellipsoid plot program. Report ORNL-5318, Oak Ridge National Laboratory, Tennessee, USA, 1976.
[27] J.R. Sambrano, A.R. de Souza, J.J. Queralt, M. Oliva, J. Andrés, Chem. Phys. 264 (2001) 333.
[28] M. Shehalatha, C. Ravikumar, I. Huber Joe, N. Sekar, V.S. Jayakumar, Spectrochim. Acta A 72 (2009) 654.
[29] M. Szafran, A. Komasa, E.B. Adamska, J. Mol. Struct. (Theochem.) 827 (2007) 101.
[30] V. Arjunan, M. Kalaivani, S. Senthilkumari, S. Mohan, Spectrochim. Acta A 115 (2013) 154.
[31] L.P. Avendaño Jiménez, G.A. Echeverría, O.E. Piro, S.E. Ulic, J.L. Jios, J. Phys. Chem. A 117 (2013) 2169.
[32] C. Sridevi, G. Shanthi, G. Velraj, Spectrochim. Acta A 89 (2012) 46.
[33] N. Sundaraganesan, G. Mariappan, S. Manoharan, Spectrochim. Acta A 87 (2011) 67.
[34] T.S. Xavier, I. Huber Joe, M.A. Palafox, S. Kumar, V.K. Rastogi, Spectrochim. Acta A 114 (2013) 502.
[35] D. Sajan, Y. Erdogdu, R. Reshmy, Ö. Dereli, K. Kurien Thomas, I. Huber Joe, Spectrochim. Acta A 82 (2011) 118.
[36] K.C. Mariamma, H.T. Varghese, C. Yohannan Panicker, K. John, J. Vinsova, C. Van Alsenoy, Spectrochim. Acta A 112 (2013) 161.
[37] V. Arjunan, S. Sakiladevi, T. Rani, C.V. Mythili, S. Mohan, Spectrochim. Acta A 88 (2012) 220.
[38] S.P.V. Chamundeeswari, E.R.J.J. Samuel, N. Sundaraganean, Eur. J. Chem. 2 (2011) 136.
[39] P. Prabavathi, A. Nilufer, V. Krishnakumar, Spectrochim. Acta A 114 (2013) 449.